

1 **Computer vision for assessing species color pattern variation from web-based community**
2 **science images**

3

4 Maggie M. Hantak^{1,4*}, Robert P. Guralnick¹, Alina Zare², Brian J. Stucky^{1,3}

5

6 ¹Florida Museum of Natural History, University of Florida, Gainesville, FL 32611, USA

7

8 ²Department of Electrical, and Computer Engineering, University of Florida, Gainesville, FL
9 32611 USA

10

11 ³Agricultural Research Service, U.S. Department of Agriculture, Beltsville, MD 20705, USA

12

13 ⁴Lead contact

14

15 *Correspondence: Maggie Hantak, Email: maggiehantak@gmail.com

16

17

18

19

20

21

22

23

24

25

26

27

28

29

30

31

32

33

34

35

36

37

38

39

40

41 **Summary**

42 Openly available community science digital vouchers provide a wealth of data to study
43 phenotypic change across space and time. However, extracting phenotypic data from these
44 resources requires significant human effort. Here, we demonstrate a workflow and computer
45 vision model for automatically categorizing species color pattern from community science
46 images. Our work is focused on documenting the striped/unstriped color polymorphism in the
47 Eastern Red-backed Salamander (*Plethodon cinereus*). We used an ensemble convolutional
48 neural network model to analyze this polymorphism in 20,318 iNaturalist images. Our model
49 was highly accurate (~98%) despite image heterogeneity. We used the resulting annotations to
50 document extensive niche overlap between morphs, but wider niche breadth for striped morphs
51 at the range-wide scale. Our work showcases key design principles for using machine learning
52 with heterogeneous community science image data to address questions at an unprecedented
53 scale.

54

55 **Introduction**

56 Species color patterns represent model systems for understanding evolution because color is a
57 quantifiable biological trait that provides pertinent information about the organism. For instance,
58 color patterns are used as a signal in mate choice and predator-prey interactions, and can aid in
59 thermoregulation (Endler and Mappes, 2017). Color polymorphic species, in which multiple
60 phenotypes (i.e., color morphs) coexist within the same population (Ford, 1945), make
61 particularly good models for studying evolutionary change, as color patterns are discrete, and
62 color morph frequency often varies geographically (McLean and Stuart-Fox, 2014). Further,
63 morphs comprise correlated trait complexes, resulting in divergent selective pressures for a
64 single species (Sinervo and Svenson, 2002; Mckinnon and Pierotti, 2010).

65 A wealth of information regarding species color patterns exists in web-based community
66 science platforms, in which contributors can upload their own photographs of animals and plants,
67 and seek help from other participants in identifying their observations. One of the largest and
68 most successful platforms is iNaturalist (<http://www.inaturalist.org/>), which as of January 2022,
69 holds > 88 million images of various species from across the world and roughly doubles in size
70 each year. DiCecco et al. (2021) showcase the research value of iNaturalist, but one still nascent
71 application is broad-scale assembly of color pattern data (but see Lehtinen et al., 2020; Lattanzio
72 and Buontempo, 2021). The key challenge is that manual extraction of color pattern data is time
73 and effort intensive. Automation is an obvious next step but complex image backgrounds can
74 confuse simplistic image analysis toolkits (Peña et al., 2014; Pollicelli et al., 2020). Therefore,
75 developing best practices and tools for streamlining extraction of information from variable
76 quality images submitted by amateur naturalists is a critical need for processing the plethora of
77 digital image data now being generated, enabling data-intensive research efforts in the areas of
78 ecology and evolutionary biology (Weinstein, 2018; Lürig et al., 2021).

79 Artificial intelligence methods, and deep learning in particular, offer the most promise for
80 automating collection of phenotypic data (Lürig et al., 2021), given their remarkable ability to

81 make accurate predictions. Convolutional neural networks (CNNs) are the basis for current state-
82 of-the-art accuracy in whole image classification (Deng et al., 2009; Zeiler, 2014; Sermanet et
83 al., 2014). A CNN is a deep learning algorithm that uses training data to learn how to extract
84 features from input images and then use those features to interpret an image's content (LeCun et
85 al., 2015). Much recent work using CNNs for ecological studies has focused on species
86 identification from complex images (e.g., camera-trap images; Wäldchen and Mäder, 2018;
87 Tabak et al., 2019; Willi et al., 2019; Whytock et al., 2021). Less developed are deep learning
88 approaches that score quantitative traits of interest on those images.

89 Here, we present a workflow and machine learning approach for classifying color
90 patterns of animals from community science photographs. To illustrate the value of this
91 computer vision model, we focus on a use-case of a striped/unstriped color pattern
92 polymorphism in the geographically widespread and abundant Eastern Red-backed Salamander,
93 *Plethodon cinereus* (Petranka, 1998). The 'striped' color morph exhibits a stripe that varies in
94 color from yellow to dark red, which is overlaid on a black dorsum, and the 'unstriped' morph is
95 completely dark in dorsal coloration (Fig. 1). The ecological and evolutionary mechanisms
96 influencing the geographic patterns of coloration in *P. cinereus* color morphs remains unclear,
97 and little work has been done to examine range-wide patterns of the polymorphism (but see
98 Gibbs and Karraker, 2006; Moore and Ouellet, 2015; Cosentino et al., 2017). Studies from single
99 populations have suggested that the color morphs are correlated with distinct climatic niches; the
100 striped morph is more associated with cooler, wetter niches, while the unstriped morph is more
101 associated with warmer, drier conditions (Moreno, 1989; Anthony et al., 2008).

102 The goal of our study was to test range-wide color morph and climate associations by
103 leveraging more than 20,000 community science photographs. We created a computer vision
104 model for scoring striped and unstriped color morphs of *P. cinereus* via an experimental design
105 capable of handling photographs that are highly heterogeneous and vary extensively in quality.
106 With the classified data, we then used ecological niche modeling and a logistic modeling
107 framework to examine whether the two color morphs partition available niche space, thereby
108 contributing to the maintenance of this polymorphism. Our methodological approach not only
109 provides new insight into the association between climate and color morph frequency in *P.*
110 *cinereus* at the range-wide scale, but also demonstrates a pipeline for rapidly classifying discrete
111 color morphs in community science images. We also discuss the complications faced when
112 developing the computer vision model, but highlight the utility of this approach with
113 continuously growing community science image resources.

114

115 **Methods**

116 *Community Science Image Dataset*

117 We downloaded 15,777 research-grade (georeferenced observations with species ID verified by a
118 minimum of two separate reviewers) images of *P. cinereus* from iNaturalist (accessed August 5,
119 2020) via a command-line query tool (https://gitlab.com/stuckyb/cbg_phenology). Images were
120 not modified in any manner. From this initial set, we randomly selected 4,000 images to be the

121 basis of our training and validation dataset. Seven volunteers aided in scoring salamander color
122 pattern (striped/unstriped). A color pattern scoring guide and training was provided by MMH to
123 all participants prior to scoring to ensure unanimity in trait definitions. Images were divided into
124 10 sets of 400. All image sets were scored twice by separate volunteers (i.e., no volunteer scored
125 the same image twice). If there was incongruence between volunteers in scoring a color pattern,
126 a third, independent, volunteer provided a consensus score.
127



128
129 **Figure 1. Color morphs of *Plethodon cinereus*.** Representative iNaturalist images of the striped (left) and unstriped
130 (right) color morphs of *Plethodon cinereus*. Photos and observations by iNaturalist users Jessica (iNaturalist user
131 jessicapfund) and Myvanwy (iNaturalist user acuriousmagpie), respectively.
132

133 To score salamander color patterns, we used the scriptable desktop software program
134 ImageAnt (<https://gitlab.com/stuckyb/imageant>). We wrote a custom ImageAnt script to query:
135 1) the number of salamanders in an image; 2) salamander color pattern (striped, unstriped, other);
136 or 3) whether the image was unusable (i.e., the color pattern was unidentifiable). Images with
137 multiple salamanders were subsequently presented with another scoring rubric of “striped”,
138 “unstriped”, or “both color morphs”. In the final training set, images with multiple of the same
139 color morph were lumped with images of a single salamander of the same color morph. Images
140 that contained both color morphs were not included in the training set. Although *P. cinereus*
141 displays a discrete striped/unstriped dorsal color pattern polymorphism, aberrant phenotypes
142 (e.g., leucistic or the orange-red “erythristic” phenotype) can be found (Moore and Ouellet,
143 2014). The few cases of erythristic (“other”) phenotypes were included within the “striped”
144 class, while no leucistic examples were observed in our training set. Our final model was trained
145 using the binary categories: “striped” and “unstriped”.
146

147 *Deep Learning*

148 We trained a convolutional neural network (CNN) using the EfficientNet (efficientnet-b4; Tan
149 and Le, 2019) architecture implemented in PyTorch with PyTorch Lightning used to implement
150 model training (Falcon, 2019). We implemented transfer learning (Yosinski et al., 2014) with
151 model weights that were pre-trained on the ImageNet dataset (Deng et al., 2009). CNN training

152 and validation was performed on the University of Florida HiPerGator high-performance
153 computer using one GPU.

154 A series of model training hyperparameters were included and systematically modified to
155 increase validation accuracy. To train the model, we used stochastic gradient descent with
156 momentum and a dynamic learning rate scheduler starting with a learning rate of 0.001 and set to
157 decay by a factor of 0.1 based on validation loss. An oversampling procedure was implemented
158 due to unequal image representation of the striped and unstriped salamander phenotypes. Image
159 preprocessing included resizing images to 596x447 pixels and normalizing the color channels
160 with the same transformation used for ImageNet pretraining. A set of data augmentation
161 techniques was applied to each batch during model training including: 1) random horizontal
162 flips, 2) random vertical flips, 3) random rotations, 4) color jittering, and 5) random affine
163 transforms.

164 We used k-fold cross-validation with 4 random splits to evaluate model performance. For
165 our final production model, we took the best model from each cross-validation fold (as defined
166 by the lowest validation loss for that fold) and combined them into an ensemble model by
167 averaging the predictions of all four models. Using ImageAnt, we manually scored 500 more
168 images that were independent of those used for model training and validation to serve as a test
169 set for evaluating the final ensemble model. We then used the production ensemble model to
170 analyze all remaining *P. cinereus* images on iNaturalist. Due to the growth of *P. cinereus*
171 research-grade images between model training and validation steps, we re-downloaded all
172 research-grade images from iNaturalist (20,318 images; accessed March 24, 2021) and then
173 analyzed all images not included in the training and test sets using the full model ensemble. Full
174 modeling details and code can be found on our GitHub repository
175 (https://github.com/mhantak/Salamander_image_analysis).
176

177 *Environmental Data*

178 To test climatic niche differences between the color morphs of *P. cinereus*, we first obtained
179 bioclimatic (n = 19) and elevational data at 30 arc-second (~1 km) resolution (WorldClim V1.4;
180 Hijmans et al., 2005). We next determined the accessible area for *P. cinereus* by buffering the
181 known geographic range by 100 km and then clipped environmental data layers to that area.
182 After doing so, and to avoid overparameterization and multicollinearity, the environmental data
183 layers were reduced to include only uncorrelated variables ($r = .80$). The final dataset included
184 eight variables: elevation, mean diurnal range (BIO2), maximum temperature of warmest month
185 (BIO5), temperature annual range (BIO7), mean temperature of wettest quarter (BIO8), mean
186 temperature of driest quarter (BIO9), precipitation seasonality (BIO15), and precipitation of
187 warmest quarter (BIO18).
188

189 *Niche Modeling*

190 We used ecological niche modeling (ENM) as a means to determine niche characteristics of both
191 morphs. Prior to running niche models, we first filtered the iNaturalist data records. Filtering

192 included removing records with missing or incomplete latitude and longitude information,
193 duplicate records, and manually removing records outside of the known range. To reduce the
194 potential for spatial autocorrelation and bias from areas with particularly dense sampling, we
195 thinned our data to include records separated by a minimum of 25 kilometers. ENM's were
196 constructed separately for both the striped and unstriped morphs using the maximum entropy
197 algorithm implemented in MAXENT V3.4.1 (Phillips et al., 2006) in the R package *ENMeval*
198 (Muscarella et al., 2014). Data were partitioned using the “block” method to account for spatial
199 autocorrelation. Regularization multipliers ranged from 0.5 to 5 and possible feature
200 combinations were: L, H, LP, LQ, LQH, LQP, and LQPH (L = linear, H = hinge, P = product, Q
201 = quadratic). The best model was selected based on the lowest $\Delta AICc$. After model calibration
202 and validation, we converted the modeled output of predicted probabilities of presence within the
203 accessible area to binary presence/absence maps using equate entropy and the original
204 distribution (cloglog) threshold, which typically performs well when attempting to balance
205 omission error versus the fraction of predicted presence. We next examined niche overlap
206 between the two morphs with the Schoener's *D* metric using *ENMeval*. Niche breadth of both
207 morphs was calculated using the raster.breadth function in the R package ENMTools (Warren et
208 al., 2010). To visually examine color morph overlap in association with climatic predictors, we
209 ran a principal component analysis (PCA) using the reduced set of bioclimatic variables and the
210 predicted presence points from the striped and unstriped morph ENM's with the base R `prcomp()`
211 function (R Core Team, 2019).

212

213 *Statistical Analyses*

214 We further quantified niche differences between the morphs by running a multiple logistic
215 regression using the R base `glm()` function (R Core Team, 2019) with a binomial family and a
216 logit link function. The predictors for this model were generated by assembling underlying
217 bioclimatic conditions (e.g., BIO2, BIO5, BIO7, BIO8, BIO9, BIO15, BIO18) and elevation at
218 each pixel predicted as a presence in the above binarized maps, for both morphs. We opted to use
219 the raw environmental data rather than principal components for ease of interpretation. Color
220 morph, coded as 1 for striped morphs and 0 for unstriped morphs was the response variable. All
221 predictors were mean-centered and scaled. In order to select the best model, and given no *a*
222 *priori* hypotheses about the best predictors, we used the ‘dredge’ function in the R package
223 *MuMIn* (Barton, 2012) to rank and assess the best-fit model with $AICc$. If any predictors were
224 not in the top model or if any predictor variance inflation factor (VIF) was greater than four, we
225 dropped those variables and re-ran the logistic regression. To generate a pseudo- R^2 value, as a
226 measure of goodness of fit for our best-fit model, we used the ‘`r2_nagelkerke`’ function in the R
227 package *performance* (Lüdecke et al., 2021).

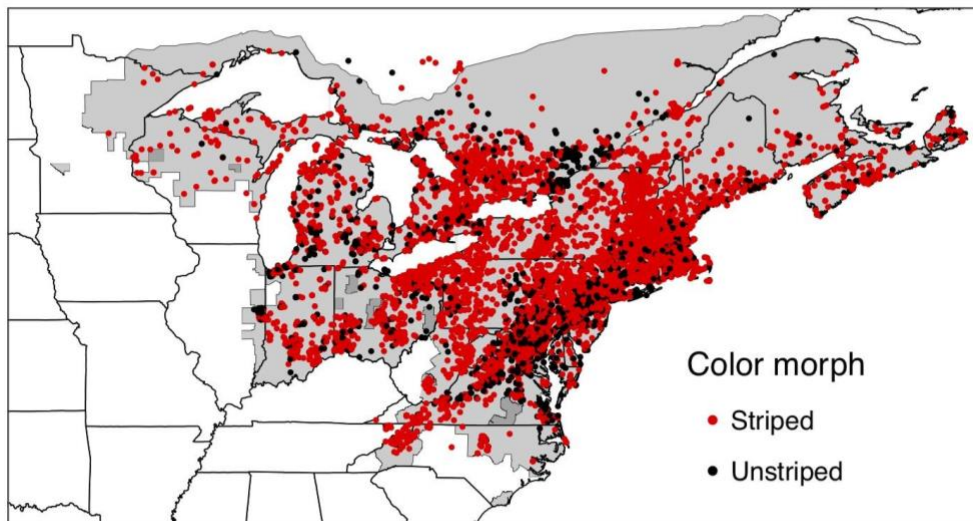
228

229 **Results**

230 *Volunteer and Model Accuracy*

231 Across the seven volunteers that scored the 4,000 training and validation images, we estimate
232 that mean volunteer annotation accuracy was 95.9%. Consensus was achieved for 3,871 (3,005
233 striped, 866 unstriped) images, while the remaining 129 images were either unidentifiable as
234 striped or unstriped salamanders (n=51) or unusable because both morphs were visible in the
235 image (n=78; Table 1). The majority of images were scored with a mean scoring time of three
236 seconds. Some images took annotators considerably longer to analyze, although extremely long
237 annotation times were likely due to annotators leaving ImageAnt running while not actively
238 scoring. The 3,871 images served as the basis for model training and validation.

239 Validation accuracy across the four cross-validation folds varied minimally (fold 1 =
240 98.6%; fold 2 = 97.3%; fold 3 = 96.2%; fold 4 = 97.4%). The mean cross-validation accuracy
241 was 97.4% and the test accuracy of the final ensemble model was 97.8% (Table 1). Out of the
242 20,318 iNaturalist images analyzed by the ensemble model, 15,413 (75.9%) were labeled as
243 striped and 4,905 (24.1%) as unstriped salamanders (Table 1)

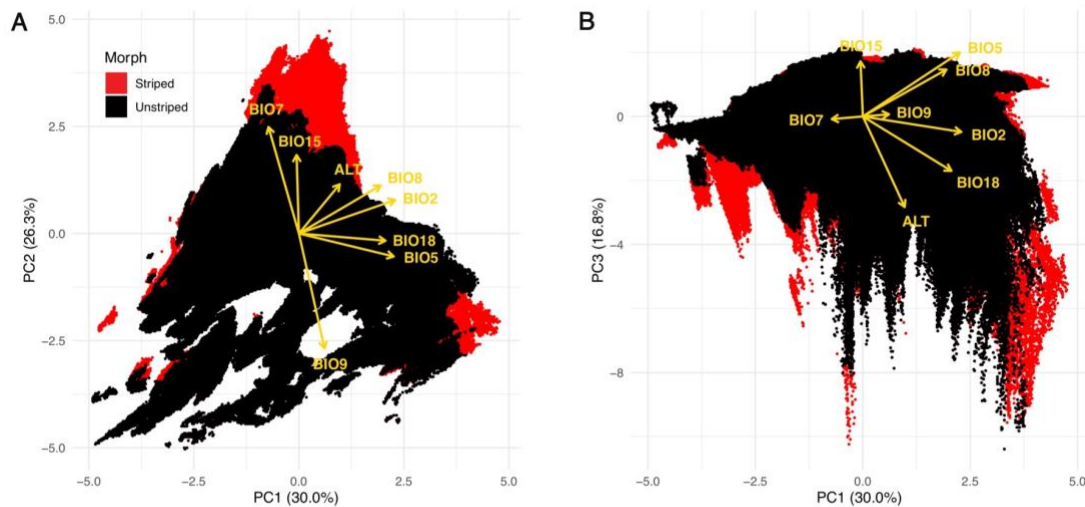


244 **Figure 2. Color morph data generated from the computer vision model.** Georeferenced iNaturalist observations
245 (N = 20,258) of *P. cinereus*. Record localities are colored by morph (red = striped, black = unstriped) based on the
246 final computer vision model run.
247

248 *Niche Modeling*

249 Our filtering steps removed 60 data points, generating a final dataset of 20,258 total point
250 presences (N = 15,363 striped morphs; N = 4,895 unstriped morphs; Fig. 2). These were used
251 along with the uncorrelated environmental predictors to generate a best-fit MAXENT model for
252 striped and unstriped morphs. The best model for both striped and unstriped, based on AICc and
253 Δ AICc, consisted of LQPH features with a regularization multiplier of two (striped model AICc
254 = 28877.63, Δ AICc = 4.86; unstriped model AICc = 16072.40, Δ AICc = 6.09). AUC_{train} (striped
255 0.78; unstriped 0.82) suggests relatively performant models; because *P. cinereus* is widespread
256 and common across its range, separating higher and lower quality habitat is more challenging
257

258 than for habitat specialists. AUC_{test} values (striped 0.75; unstriped 0.81) were close to the
259 AUC_{train} scores, suggesting these models are not overfit. The Schoener's D metric indicates that
260 the niches of the morphs overlap at 87%. Niche breadth of the striped morph is greater than that
261 of the unstriped morph (Levins B_2 ; striped = 0.64; unstriped = 0.55). The PCA of the reduced
262 bioclimatic variables shows how the morphs partition niche space (Table S1, Fig. 3). PC1
263 represents 30% of the variation and its loadings are primarily mean diurnal range (BIO2),
264 maximum temperature of warmest month (BIO5), and precipitation of warmest quarter (BIO18;
265 Fig 3A). PC2 represents 26% of the variation and mean temperature of driest quarter (BIO9),
266 temperature annual range (BIO7), and precipitation seasonality (BIO15; Fig. 3A) are the main
267 loadings. Lastly, 17% of the variation is explained by PC3, with loadings primarily from
268 elevation (ALT) and maximum temperature of warmest month (BIO5; Fig. 3B).
269

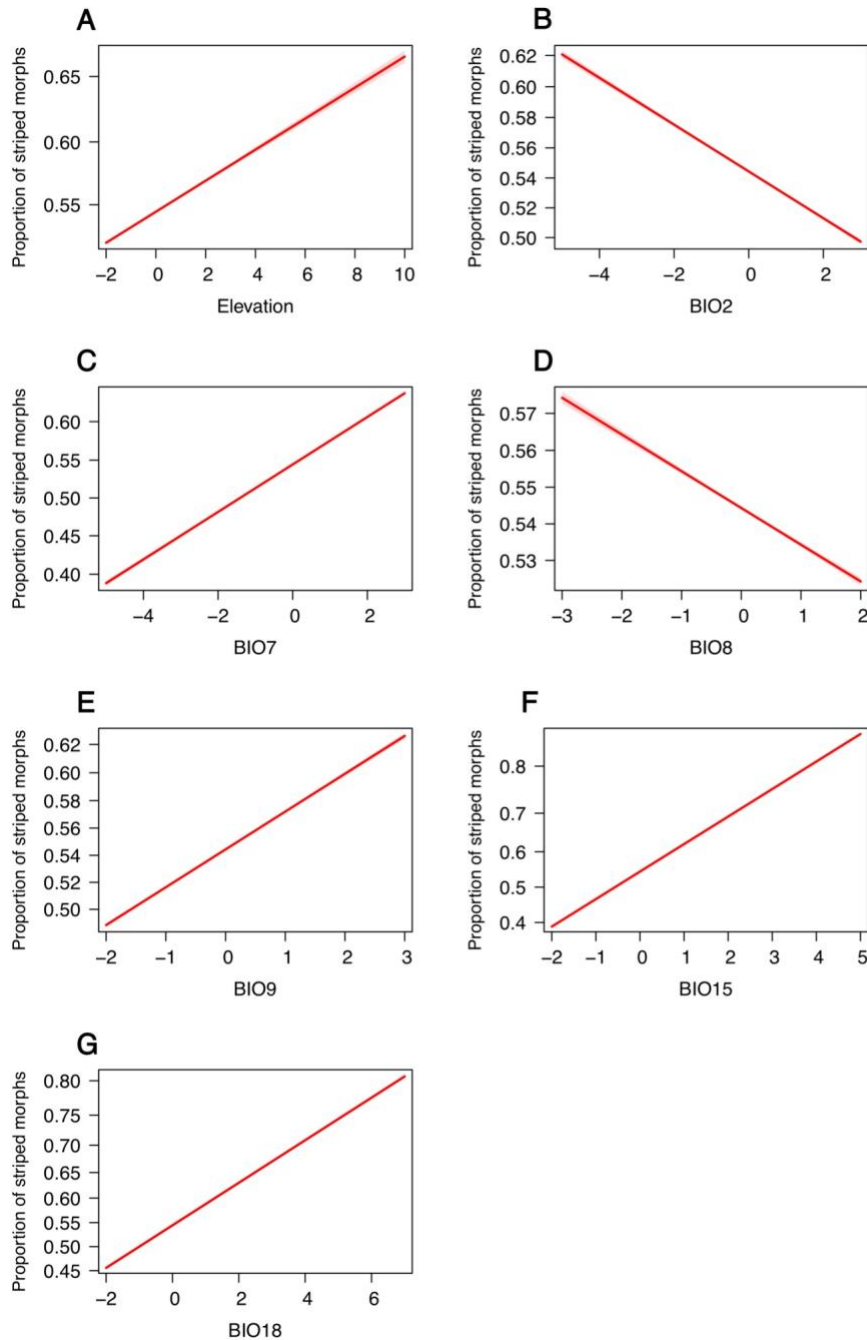


270
271 **Figure 3. Climatic niche differences between color morphs of *Plethodon cinereus*.** PCA of reduced climatic
272 variables: A) PC1-PC2, B) PC1-PC3. Predicted presence points from striped and unstriped morph ecological niche
273 models were grouped into hexbins (red = striped; black = unstriped). PCA loadings are represented by yellow
274 arrows.

275 276 *Logistic Modeling*

277 The best model included elevation and all seven bioclimatic predictors (BIO2, BIO5, BIO7,
278 BIO8, BIO9, BIO15, BIO18), however, BIO5 was subsequently dropped because it had a VIF
279 greater than four ($PseudoR^2 = 0.04$). All model effects were significant. Striped morph frequency
280 is positively correlated with elevation ($\beta = 0.051$, $SE = 0.001$, $p < 0.001$; Fig. 4A). There is a
281 decreased odds of striped morphs with mean diurnal range (BIO2; $\beta = -0.063$, $SE = 0.001$, $p <$
282 0.001 ; Fig. 4B). Striped morph frequency has higher odds of occurring with higher temperature
283 annual range (BIO7; $\beta = 0.126$, $SE = 0.001$, $p < 0.001$; Fig. 4C), but the odds decrease with mean
284 temperature of the wettest quarter (BIO8; $\beta = -0.040$, $SE = 0.001$, $p < 0.001$; Fig. 4D). The odds
285 of striped morph frequency increases with mean temperature of driest quarter (BIO9; $\beta = 0.112$,

286 $SE = 0.001, p < 0.001$; Fig. 4E) and with both precipitation predictors: precipitation seasonality
287 (BIO15; $\beta = 0.315, SE = 0.001, p < 0.001$; Fig. 4F) and precipitation of the warmest quarter
288 (BIO18; $\beta = 0.178, SE = 0.001, p < 0.001$; Fig. 4G). Precipitation effect sizes were generally
289 stronger than temperature in separating morphs.
290



291
292 **Figure 4. Climatic predictors of color morph frequency.** Top model effect plots of color morph frequency
293 variation in *P. cinereus*. The proportion of color morphs is influenced by A) elevation; B) mean diurnal range
294 (BIO2); C) temperature annual range (BIO7); D) mean temperature of wettest quarter (BIO8); E) mean temperature

295 of direct quarter (BIO9); F) precipitation seasonality (BIO15); and G) precipitation of warmest quarter (BIO18).
296 95% confidence intervals are included in each plot.

297

298 **Discussion**

299 Community science resources, especially images tied to community identifications available via
300 iNaturalist, are rapidly expanding. These images contain a treasure trove of biologically relevant
301 information about phenotypes and interactions (DiCecco et al., 2021), but unlocking this
302 information remains a challenge. Thus far, computer vision models have largely focused on
303 species identification from images (Gomez Villa et al., 2017; Norouzzadeh et al., 2018; Willi et
304 al., 2019). To our knowledge, no previous studies have aimed to use machine learning
305 approaches to extract trait information, but such approaches are needed given the deluge of
306 records with digital vouchers being submitted. Here, we created a highly accurate (~98%
307 accurate based on test set evaluation) computer vision model for classifying a salamander's color
308 pattern from community science images. With the data produced from this model, we expanded
309 our knowledge of why a common striped/unstriped color polymorphism persists in the abundant
310 salamander, *Plethodon cinereus*.

311

312 *Scalability of Community Science Images*

313 A challenge of using CNNs for feature classification is the need for robust sample sizes for
314 training. Community science platforms, such as iNaturalist, hold millions of images of various
315 plants and animals that are spatially and temporally replicated. A well-established machine
316 learning algorithm provides iNaturalist users with a suggested species identification
317 (www.inaturalist.org/). A few studies have manually scored traits such as flower presence or
318 absence in order to identify phenological patterns across geography (Barve et al., 2020; Li et al.,
319 2021). Yet, manual scoring of more images would be necessary to expand upon these studies.
320 Our pipeline provides a streamlined example of how to obtain large-scale trait data from
321 community science images. This computer vision model can now be used to rapidly score the
322 trait of interest, and can be used in perpetuity to gather data on more records as they become
323 available on community science platforms. From August 5th, 2020 when we downloaded our
324 core image dataset used for model training to January 13th, 2022, the number of research-grade
325 *P. cinereus* records has nearly doubled (from 15,777 to 29,040). As well, many other *Plethodon*
326 species have similar color polymorphisms and our model should be transferable to these other
327 species.

328 Community science images are not perfect. With unstandardized images, expert decisions
329 on feature classifications are key. For this work, we created a salamander color scoring guide
330 (found in https://github.com/mhantak/Salamander_image_analysis) that was distributed to all
331 volunteers who aided in creating the training dataset. While standardization of training data is
332 important, some aspects of community science images remain out of our control and create
333 unique challenges when designing machine learning experiments. For instance, during volunteer
334 scoring, there were a few research-grade species misidentifications, which is unsurprising given
335 that closely related species can look nearly identical to *P. cinereus* (Fisher-Reid and Wiens,

336 2015). These sorts of issues are inherent in working with community science data, but careful
337 consideration is needed when making decisions about how to deal with these records. In our
338 case, we scored misidentified species to the most similar looking morph of *P. cinereus*. For
339 example, a Two-lined Salamander (*Eurycea* sp.), was categorized as a striped morph, while a
340 Slimy Salamander (*Plethodon glutinosus*) was scored as an unstriped morph. Keeping these
341 images of similar-looking species in the training dataset provides a more representative sample
342 of what the model will encounter when analyzing new images. Further, there were several
343 images solely of the ventral side of the salamander. While not a misidentification, the needed
344 trait information is best obtained from a dorsal view, and ventral views would be better suited as
345 additional images to augment iNaturalist records that also include a dorsal view. Due in part to
346 these ventral images, there were 51 images out of 4,000 (1.3%) that were excluded from the
347 training dataset because they could not be identified to morph. Other image problems included
348 excessive blurriness, partial body part exposure (e.g., head only), or a salamander that was too
349 distant in the photograph. Even if ~1% of all input images are unidentifiable and the model were
350 to incorrectly guess on all of them, we maintain that this is still an acceptable error rate when
351 dealing with community science images. Finally, we removed one extraneous data point from the
352 data after determining it was well outside of the geographic range of the species. One record out
353 of >20,000 is a very low error rate.

354

355 *Computer Vision Model Intricacies*

356 Our final computer vision model is based on a binary classification, ‘striped’ or ‘unstriped’ color
357 morph. This simplified binary classifier works for the majority of individual *P. cinereus* across
358 the distribution of the species. However, there is a third, uncommon erythristic (orange-red)
359 color morph, which we combined with the striped morph (similar to another study; Fisher-Reid
360 and Wiens, 2015) because there were too few examples in our training image set ($n = 20$) to train
361 a model to identify it. In addition, other abnormal color phenotypes of *P. cinereus* can sometimes
362 be found (see Moore and Ouellet, 2014). When preparing our training dataset, we found 16
363 instances of a white (instead of orange or red) striped phenotype. As with the erythristic
364 phenotype, these images were too sparse for model training and were lumped with striped
365 morphs based on the existence of the dorsal stripe. Similar decisions were necessary for less
366 frequent aberrant phenotypes. Single images that contained multiple salamanders also posed an
367 issue with creating our training set. We initially considered attempting to train a model to
368 determine the number of salamanders in an image or identify images with multiple salamanders.
369 However, a stepwise classifier would require more training images for the additional categories
370 and ultimately create a more unbalanced dataset, as there were less images with multiple
371 salamanders. We, thus, adopted the simple solution of combining images with multiple
372 salamanders of the same phenotype with images of single salamanders (e.g., an image with three
373 striped morphs was binned into the “striped” class). We removed images that contained both
374 color morphs from the training set because *either* category (striped or unstriped) could be
375 considered correct for these images. At inference time, images with both color morphs were

376 considered to be correctly classified regardless of which color morph the model assigned them.
377 Such images are quite rare and accounted for only 78 of the 4,000 images analyzed to generate
378 the training and test sets.

379

380 *Climate & Color Morph Trends in the Eastern Red-backed Salamander*

381 The ecological niche models show that the morphs largely overlap (i.e., by 87%) in climatic
382 niche space, but striped morphs have a wider niche breadth than unstriped morphs. The PCA
383 highlights the variation between *P. cinereus* color morphs and in general shows that striped
384 morphs can be found in areas with more variable climatic conditions. Logistic model findings are
385 consistent with the PCA and demonstrate a positive association between striped morph frequency
386 and elevation, metrics of precipitation, and two climate variables (BIO7 and BIO9). Whereas the
387 proportion of striped morphs decreases with mean diurnal range (BIO2) and mean temperature of
388 wettest quarter (BIO8).

389 Our finding of a positive relationship between elevation and striped morph frequency is
390 consistent with previous studies (Gibbs and Karraker, 2006; Moore and Ouellet, 2015; Hantak et
391 al., 2021). Following the expectation that higher elevations are typically colder than lower
392 elevations, we predicted the observed positive correlation. However, here and in other studies,
393 striped morphs are not always associated with cooler temperatures. A recent study by Hantak et
394 al. (2021) found the proportion of striped morphs increases with increasing elevation and mean
395 annual temperature and, based on these results suggested that these predictors may be decoupled
396 in relation to color morph frequency in *P. cinereus*. While the reason for greater proportion of
397 striped morphs in higher elevations remains unclear, it may be possible that gene flow is reduced
398 along altitudinal gradients in this species. Previous work has shown that elevation is a significant
399 predictor of genetic differentiation in amphibians (Funk et al., 2005; Giordano et al., 2007;
400 García-Rodríguez et al., 2021), including *P. cinereus* (Hantak et al., 2019); although moderate
401 changes in elevation was not the most important driver of morph frequency variation in northern
402 Ohio (Hantak et al., 2019).

403 Based on previous studies of climate associations between in *P. cinereus* color morphs,
404 we predicted that striped morph occurrences would be more tightly linked with cooler and wetter
405 climatic niches, whereas unstriped morphs would be more correlated with warmer, drier niches
406 (Lotter and Scott, 1977; Moreno, 1989; Anthony et al., 2008). While we found the predicted
407 trend for precipitation with striped morph frequency, our temperature-morph findings were more
408 nuanced. The PCA and logistic model indicates that the striped morph is, in general, found in
409 areas with more variability in temperature. Whereas the proportion of striped morphs decreases
410 with mean diurnal range (BIO2), suggesting that striped morphs are negatively impacted by
411 temperature fluctuations. In addition, the proportion of striped morphs decreased with mean
412 temperature of wettest quarter (BIO8), indicating a possible humidity threshold for this morph.

413 Much work on the polymorphism in *P. cinereus* relies heavily on findings that were
414 conducted over relatively small spatial and temporal scales. In addition, some studies have found
415 no climate-related morph trends or inconsistent patterns over time (Petruzzini et al., 2006; Muñoz

416 et al., 2016; Evans et al., 2018). Fisher-Reid et al. (2013) demonstrated that striped morphs were
417 found in warmer, wetter habitats on Long Island, New York, while Hantak et al. (2021) found
418 striped morphs were more associated with warmer, drier habitats in localities across Maryland,
419 New York, and Virginia. Range-wide, dense data can help examine overall trends and localize
420 those at finer scale in a unifying framework. Besides our current work, two other studies have
421 attempted to examine climate-morph trends in *P. cinereus* across a greater proportion of the
422 species range. But here again, these studies find conflicting results likely due to differences in
423 datasets, covariates, and statistical approaches (Gibbs and Karraker, 2006; Moore and Ouellet,
424 2015; Cosentino et al., 2017). It is possible that these variations in approaches lead to ambiguous
425 color morph and climate relationships, or it may be there are more complex contextual cues that
426 are being missed when attempting to understand polymorphism rates in *P. cinereus*. With
427 physiological differences between the morphs (Moreno, 1989; Davis and Milanovich, 2010;
428 Smith et al., 2015), climate likely plays some role in morph distribution, but other, local,
429 selection pressures may be more important in this system.

430

431 *Next Steps*

432 The combination of community science and deep learning provides a powerful resource for
433 future studies of phenotypic variation. With the rapid growth of data, including community
434 science images, scalable resources such as computer vision models are necessary to keep pace
435 with rate of data accumulation (Hassoun et al., 2021), which potentially provides a means to
436 track temporal changes, not simply spatial ones. A further step for our research is to use this
437 model to score color morphs of other species within the salamander genus *Plethodon*. In total,
438 there are 10 species within *Plethodon* that contain the exact same dorsal striped/unstriped color
439 pattern (Petranka, 1998; Highton, 2004). Occurrence data points are available for all of these
440 other species on the iNaturalist platform, ranging from ~70 observations for the IUCN listed
441 “vulnerable” mountaintop endemic, *P. sherando* (Highton and Collins, 2006) to >2,000
442 observations of the more widespread Western Red-backed Salamander (*P. vehiculum*). Much
443 research has been done on the morphs of *P. cinereus*, but very little is known about dynamics of
444 the polymorphism in these other species, including whether the morphs diverge in climatic niche
445 space. Although our computer vision model was developed to score salamander striped and
446 unstriped color patterns, our entire workflow can also be transferred to any system that has
447 discrete, easily identifiable, trait variation.

448

449 *Limitations of the Study*

450 Although machine learning holds much promise for rapidly gathering phenotypic data from
451 digital images, the main limitation to using fully supervised deep learning approaches is the
452 number of labeled training images (and, primarily, the time and expertise needed to generate the
453 labels). Depending on the complexity of the intended classification, several thousand vouchers
454 for each category may be necessary for training and validating the model. Here, we present a
455 relatively simple problem: are the salamanders striped or unstriped? Adding categories or

456 addressing more complicated phenotypes will require more training images. In the deep learning
457 literature, methods to reduce the labeling bottleneck (e.g., through one- or few-shot learning;
458 O'Mahony et al. 2019; Wang et al. 2020) are being developed and future studies on the
459 applicability and effectiveness of those methods to the application presented here are needed.
460 The other main limitation to the type of work we presented in this paper is the imperfect nature
461 of community science images. Misidentifications do occur, even when reducing the dataset to
462 vetted (e.g., research-grade) images, and images themselves vary in absolute quality and relative
463 usability for a particular trait scoring outcome. Solutions to dealing with these issues will be on a
464 case-to-case basis, but in our work, we found that labeling misidentified species to the closest
465 phenotype and filtering some of the most problematic images worked well. Misidentifications
466 and unusable images are inherent when working with community science data, but they are
467 infrequent. With tens of thousands of correctly identified images of usable quality, a few
468 misidentifications and image issues will not dramatically impact the biological conclusions of the
469 study. Certainly, future work can also include leveraging weak-learning approaches that are more
470 robust to the presence of label noise and inaccuracies.

471

472 **Resource Availability**

473 *Lead Contact*

474 Further information or requests for resources should be directed to the Lead Contact, Maggie M.
475 Hantak (maggiehantak@gmail.com)

476

477 **Data and Code Availability**

478 Data and code for this study are available at

479 https://github.com/mhantak/Salamander_image_analysis.

480

481 **Acknowledgements**

482 We thank iNaturalist community science users for their efforts in documenting and identifying
483 Eastern Red-backed Salamander occurrences. We also thank volunteers N. Barve, V. Barve, N.
484 Gardner, and N. Sewnath for scoring salamander color patterns, which were used in the training
485 dataset. Research reported in this publication was supported by the University of Florida
486 Informatics Institute Fellowship Program and the NSF Postdoctoral Research Fellowship in
487 Biology (2010776) both awarded to MMH.

488

489 **Author Contributions**

490 MMH, RPG, AZ, and BJS designed the study. MMH and BJS developed the computer vision
491 model. Ecological analyses were led by MMH and RPG. MMH wrote the manuscript. All
492 authors contributed to drafts and the final version of the manuscript.

493

494 **Declaration of Interests**

495 The authors declare no competing interests.

496

497 **References**

- 498 Anthony, C. D., Venesky, M. D., and Hickerson, C. A. M. (2008). Ecological separation in a
499 polymorphic terrestrial salamander. *J. Anim. Ecol.* 77, 646–653.
500
- 501 Barton, K. (2012). Package ‘MuMIn’. Model selection and model averaging based on
502 information criteria. R package version 3.2.4. [http://cran.r-project.org/web/packages/MuMIn/](http://cran.r-project.org/web/packages/MuMIn/index.html)
503 [index.html](http://cran.r-project.org/web/packages/MuMIn/index.html).
504
- 505 Barve, V. V., Brenskelle, L., Li, D., Stucky, B. J., Barve, N. V., Hantak, M. M., McLean, B. S.,
506 Paluh, D. J., Oswald, J. A., Belitz, M. W., Folk, R. A., and Guralnick, R. P. (2020). Methods for
507 broad-scale plant phenology assessments using citizen scientists’ photographs. *Appl. Plant Sci.*
508 8, e11315.
509
- 510 Cosentino, B. J., Moore, J.-D., Karraker, N. E., Ouellet, M., and Gibbs, J. P. (2017).
511 Evolutionary response to global change: climate and land use interact to shape color
512 polymorphism in a woodland salamander. *Ecol. Evol.* 7, 5426–5434.
513
- 514 Davis, A. K., and Milanovich, J. R. (2010). Lead-phase and red-stripe color morphs of red-
515 backed salamanders *Plethodon cinereus* differ in hematological stress indices: a consequence of
516 differential predation pressure? *Curr. Zool.* 56, 238–243.
517
- 518 Deng, J., Dong, W., Socher, R., Li, L. J., Li, K., and Fei-Fei, L. (2009). ImageNet: A Large-
519 Scale Hierarchical Image Database. In 2009 IEEE Conference on Computer Vision and Pattern
520 Recognition, 248–255.
521
- 522 DiCecco, G. J., Barve, V., Belitz, M. W., Stucky, B. J., Guralnick, R. P., and Hurlbert, A. H.
523 (2021). Observing the observers: How participants contribute data to iNaturalist and implications
524 for biodiversity science. *Bioscience* 71, 1179–1188.
525
- 526 Endler, J. A., and Mappes, J. (2017). The current and future state of animal coloration research.
527 *Philos. Trans. R. Soc. Lond. B. Biol. Sci.* 372, 20160352.
528
- 529 Evans, A. E., Forester, B. R., Jockusch, E. L., and Urban, M. C. (2018). Salamander morph
530 frequencies do not evolve as predicted in response to 40 years of climate change. *Ecography*
531 41,1687–1697.
532
- 533 Falcon, W. (2019). Pytorch lightning. GitHub. Note: [https://github.com/williamFalcon/pytorch-](https://github.com/williamFalcon/pytorch-lightning)
534 [lightning](https://github.com/williamFalcon/pytorch-lightning).
535
- 536 Fisher-Reid, M. C., and Wiens, J. J. (2015). Is geographic variation within species related to
537 macroevolutionary patterns between species? *J. Evol. Biol.* 28, 1502–1515.
538
- 539 Fisher-Reid, M. C., Engstrom, T. N., Kuczynski, C. A., Stephens, P. R., and Wiens, J. J. (2013).
540 Parapatric divergence of sympatric morphs in a salamander: incipient speciation on Long Island?
541 *Mol. Ecol.* 22, 4681–4694.
542

- 543
544 Ford, E. B. (1945). Polymorphism. *Biol. Rev.* *20*, 73–88.
545
- 546 Funk, W. C., Blouin, M. S., Corn, P. S., Maxell, B. A., and Pilliod, D. S. Population structure of
547 Columbia spotted frogs (*Rana lueteiventris*) is strongly affected by the landscape. (2005). *Mol.*
548 *Ecol.* *14*, 1–14.
549
- 550 García-Rodríguez, A., Martínez, P. A., Oliveira, B. F., Velasco, J.A., Pyron, R. A., and Costa, G.
551 C. (2021). Amphibian speciation rates support a general role of mountains as biodiversity pumps.
552 *Am Nat.* *198*, E68–E79.
553
- 554 Gibbs, J. P., and Karraker, N. E. (2006). Effects of warming conditions in eastern North
555 American forests on red-backed salamander morphology. *Conserv. Biol.*, *20*, 913–917.
556
- 557 Giordano, A.R., Ridenhour, B. J., and Storfer, A. (2007). The influence of altitude and
558 topography on genetic structure in the long-toed salamander (*Ambystoma macrodactylum*). *Mol.*
559 *Ecol.* *16*, 1625–1637.
560
- 561 Gomez Villa, A., Salazar, A., and Vargas, F. (2017). Towards automatic wild animal monitoring:
562 Identification of animal species in camera-trap images using very deep convolutional neural
563 networks. *Ecol. Inform.* *41*, 24–32.
564
- 565 Hantak, M. M., Page, R. B., Converse, P. E., Anthony, C. D., Hickerson, C. M., and Kuchta, S.
566 R. (2019). Do genetic structure and landscape heterogeneity impact color morph frequency in a
567 polymorphic salamander? *Ecography* *42*, 1383–1394.
568
- 569 Hantak, M. M., Federico, N. A., Blackburn, D. C., and Guralnick, R. P. (2021). Rapid
570 phenotypic change in a polymorphic salamander over 43 years. *Sci. Rep.* *11*, 22681.
571
- 572 Hassoun, A., Jefferson, F., Shi, X., Stucky, B., Wang, J., and Rosa Jr., E. (2021). Artificial
573 intelligence for biology. *Integrative and Comparative Biology* doi.org/10.1093/icb/icab188.
574
- 575 Highton, R. (2004). A new species of woodland salamander of the *Plethodon cinereus* group
576 from the Blue Ridge Mountains of Virginia. *Jeffersoniana* *14*, 1–22.
577
- 578 Highton, R., and Collins, J. (2006). *Plethodon sherando*. The IUCN Red List of Threatened
579 Species 2006: e.T61905A12569864.
580
- 581 Hijmans, R. J., Cameron, S. E., Parra, J. L., Jones, P. G., and Jarvis, A. (2005). Very high
582 resolution interpolated climate surfaces for global land areas. *Int. J. Climatol.* *25*, 1965–1978.
583
- 584 iNaturalist. (2021). Available online: <https://www.inaturalist.org/>.
585
- 586 Lattanzio, M. S., and Buontempo, M. J. (2021). Ecogeographic divergence linked to dorsal
587 coloration in Eastern Hog-Nosed Snakes (*Heterodon platirhinos*). *Herpetologica* *77*, 134–145.
588

- 589 LeCun, Y., Bengio, Y., and Hinton, G. (2015). Deep learning. *Nature* 521, 436–444.
590
- 591 Lehtinen, R. M., Carlson, B. M., Hamm, A. R., Riley, A. G., Mullin, M. M., and Gray, W. J.
592 (2020). Dispatches from the neighborhood watch: Using citizen science and field survey data to
593 document color morph frequency in space and time. *Ecol. Evol.* 10, 1526.
594
- 595 Li, D., Barve, N., Brenskelle, L., Earl, K., Barve, V., Belitz, M. W., Doby, J., Hantak, M. M.,
596 Oswald, J. A., Stucky, B. J., Walters, M., and Guralnick, R. P. (2021). Climate, urbanization, and
597 species traits interactively drive flowering duration. *Glob. Change Biol.* 27, 892–903.
598
- 599 Lotter, F., and N. J. Scott Jr. (1977). Correlation between climate and distribution of the color
600 morphs of the salamander *Plethodon cinereus*. *Copeia* 1977, 681–690.
601
- 602 Lüdecke, D., Ben-Shachar, M., Patil, I., Waggoner, P., and Makowski, D. (2021). performance:
603 An R Package for Assessment, Comparison and Testing of Statistical Models. *J. Open Source*
604 *Softw.* 6, 3139.
605
- 606 Lürig, M., Donoughe, S., Svensson, E. I., Porto, A., and Tsuboi, M. (2021). Computer vision,
607 machine learning, and the promise of phenomics in ecology and evolutionary biology. *Front.*
608 *Ecol. Evol.* 9, 642774.
609
- 610 Mckinnon, J. S., and Pierotti, M. R. (2010). Colour polymorphism and correlated characters:
611 genetic mechanisms and evolution. *Mol. Ecol.* 19, 5101–5125.
612
- 613 McLean, C. A., and Stuart-Fox, D. (2014). Geographic variation in animal colour
614 polymorphisms and its role in speciation. *Biol. Rev.* 89, 860–873.
615
- 616 Moore, J. D., and Ouellet, M. (2014). A review of colour phenotypes of the eastern red-backed
617 salamander, *Plethodon cinereus*, in North America. *Can. Field-Nat.* 128, 250–259.
618
- 619 Moore, J. D., and Ouellet, M. (2015). Questioning the use of an amphibian colour morph as an
620 indicator of climate change. *Glob. Change Biol.* 21 566–571.
621
- 622 Moreno, G. (1989). Behavioral and physiological differentiation between the color morphs of the
623 salamander, *Plethodon cinereus*. *J. Herpetol.* 23, 335–341.
624
- 625 Muñoz, D. J., Hesed, K. M., Grant, E. H. C., and Miller, D. A. W. (2016). Evaluating within-
626 population variability in behavior and demography for the adaptive potential of a dispersal-
627 limited species to climate change. *Ecol. Evo.* 6, 8740–8755.
628
- 629 Muscarella, R., Galante, P. J., Soley-Guardia, M., Boria, R. A., Kass, J. M., Uriarte, M., and
630 Anderson, R. P. (2014). ENMeval: An R package for conducting spatially independent
631 evaluations and estimating optimal model complexity for MAXENT ecological niche models.
632 *Methods Ecol. Evol.*, 5, 1198–1205.
633
- 634 Norouzzadeh, M. S., Nguyen, A., Kosmala, M., Swanson, A., Palmer, M. S., Packer, C., and

- 635 Clune, J. (2018). Automatically identifying, counting, and describing wild animals in camera-
636 trap images with deep learning. *Proc. Natl. Acad. Sci.*, *115*, E5716–E5725.
637
- 638 O’ Mahony, N., Campbell, S., Carvalho, A., Krpalkova, L., Hernandez, G. V., Harapanahalli, S.,
639 Riordan, D., and Walsh, J. (2019). One-shot learning for custom identification tasks; A review.
640 In *Procedia Manufacturing*, Elsevier B.V.: Amsterdam, The Netherlands. Volume 38, pp. 186–
641 193.
642
- 643 Peña, J., Gutiérrez, P., Hervás-Martínez, C., Six, J., Plant, R., and López-Granados, F. (2014).
644 Object-based image classification of summer crops with machine learning methods. *Remote*
645 *Sens.* *6*, 5019.
646
- 647 Petranka, J. W. 1998. *Salamanders of the United States and Canada*. Smithsonian Press,
648 Washington.
649
- 650 Petruzzi, E. E., Niewiarowski, P. H., and Moore, F. B.-G. (2006). The role of thermal niche
651 selection in maintenance of colour polymorphism in redback salamanders (*Plethodon cinereus*).
652 *Front. Zool.* *3*, 10.
653
- 654 Phillips, S. J., Anderson, R. P., and Schapire, R. E. (2006). Maximum entropy modeling of
655 species geographic distributions. *Ecol. Modell.* *190*, 231–259.
656
- 657 Pollicelli, D., Coscarella, M., and Delrieux, C. (2020). RoI detection and segmentation
658 algorithms for marine mammals photo-identification. *Ecol. Inform.* *56*, 101038.
659
- 660 R Core Team. (2019). R: a language and environment for statistical computing. R Foundation for
661 Statistical Computing, <https://www.R-project.org/>.
662
- 663 Sermanet, P., Frome, A., and Real, E. (2014). Attention for fine grained categorization.
664 *arXiv:1412.7054*.
665
- 666 Sinervo, B., and E. Svensson. (2002). Correlational selection and the evolution of genomic
667 architecture. *Heredity* *89*, 329–338.
668
- 669 Smith, G. R., Johnson, T., Smith, W. O. (2015). Effects of colour morph and season on the
670 dehydration and rehydration rates of *Plethodon cinereus*. *Amphib-Reptil.* *36*, 170–174.
671
- 672 Tabak, M. A., Norouzzadeh, M. S., Wolfson, D. W., Sweeney, S. J., Vercauteren, K. C., Snow,
673 N. P., Halseth, J. M., Di Salvo, P. A., Lewis, J. S., White, M. D., et al. (2019). Machine learning
674 to classify animal species in camera trap images: Applications in ecology. *Methods Ecol. Evol.*
675 *10*, 585–590.
676
- 677 Tan, M., and Le, Q. V. (2019). Efficientnet: Rethinking model scaling for convolutional neural
678 networks. *arXiv 1905.11946*.
679
- 680 Wäldchen, J., and Mäder, P. (2018). Machine learning for image based species identification.

681 Methods Ecol. Evol. 9, 2216–2225.
682
683 Wang, Y., Yao, Q., Kwok, J., and Ni, L. M. (2020). Generalizing from a few examples: a survey
684 on few-shot learning. *ACM Comput. Surv.* 53, 1–34.
685
686 Warren, D. L., Glor, R. E., and Turelli, M. (2010). ENMTools: a toolbox for comparative studies
687 of environmental niche models. *Ecography* 33, 607–611.
688
689 Weinstein, B. G. (2018). A computer vision for animal ecology. *J. Animal Ecol.* 87, 533–545.
690
691 Willi, M., Pitman, R. T., Cardoso, A. W., Locke, C., Swanson, A., Boyer, A., Veldhuis, M., and
692 Fortson, L. (2019). Identifying animal species in camera trap images using deep learning and
693 citizen science. *Methods Ecol. Evol.* 10, 80–91.
694
695 Whytock, R.C., Świeszewski, J., Zwerts, J.A., Bara-Słupski, T., Pambo, A.F.K., Rogala, M.,
696 Bahaa-el-din, L., Boekee, K., Brittain, S., Cardoso, A.W., Henschel, P., Lehmann, D., Momboua,
697 B., Opepa, C.K., Orbell, C., Pitman, R.T., Robinson, H.S., and Abernethy, K.A. (2021). Robust
698 ecological analysis of camera trap data labelled by a machine learning model. *Methods Ecol.*
699 *Evol.* 12, 1080–1092.
700
701 Yosinski, J., Clune, J., Bengio, Y., and Lipson, H. (2014). How transferable are features in deep
702 neural networks? In *Advances in neural information processing systems*, Z. Ghahramani, M.
703 Welling, C. Cortes, N. D. Lawrence, and K. Q. Weinberger, Eds. (Curran Associates, Inc), pp.
704 2220–3328.
705
706 Zeiler, M. D., and Fergus. (2014). Visualizing and understanding convolutional networks. *Notes*
707 *Comut. Sci.* 8689, 818–833.
708
709
710
711
712
713
714
715
716
717
718
719
720
721
722
723
724
725
726

727 **Table**

728

729 Table 1. Total number of images and how the images were classified for different datasets. 1)

730 Volunteer scoring for the training and validation dataset. 2) Examination of a subset (500

731 images) of the final model ensemble to retrieve an estimate of model accuracy. 3) Final computer

732 vision model color pattern scores.

733

Image Dataset	Total Images	Striped	Unstriped	Incorrect/unidentifiable
Training & validating	4,000	3,005	866	129
Ensemble accuracy	500	374	115	11
Final output	20,318	15,413	4,905	NA

734

735

736

737

738

739

740

741

742

743

744

745

746

747

748

749

750

751

752

753

754

755

756

757

758

759

760

761

762

763 **Figure Legends**

764

765 **Figure 1. Color morphs of *Plethodon cinereus*.** Representative iNaturalist images of the striped
766 (left) and unstriped (right) color morphs of *Plethodon cinereus*. Photos and observations by
767 iNaturalist users Jessica (iNaturalist user jessicapfund) and Myvanwy (iNaturalist user
768 acuriousmagpie), respectively.

769

770 **Figure 2. Color morph data generated from the computer vision model.** Georeferenced
771 iNaturalist observations (N = 20,258) of *P. cinereus*. Record localities are colored by morph (red
772 = striped, black = unstriped) based on the final computer vision model run.

773

774 **Figure 3. Climatic niche differences between color morphs of *Plethodon cinereus*.** PCA of
775 reduced climatic variables: A) PC1-PC2, B) PC1-PC3. Predicted presence points from striped
776 and unstriped morph ecological niche models were grouped into hexbins (red = striped; black =
777 unstriped). PCA loadings are represented by yellow arrows.

778

779 **Figure 4. Climatic predictors of color morph frequency.** Top model effect plots of color
780 morph frequency variation in *P. cinereus*. The proportion of color morphs is influenced by A)
781 elevation; B) mean diurnal range (BIO2); C) temperature annual range (BIO7); D) mean
782 temperature of wettest quarter (BIO8); E) mean temperature of driest quarter (BIO9); F)
783 precipitation seasonality (BIO15); and G) precipitation of warmest quarter (BIO18). 95%
784 confidence intervals are included in each plot.

785

786

787

788

789

790

791

792

793

794

795

796

797

798

799

800

801

802

803

804

805 **Supplemental Information**

806

807 Supplemental Table 1. PCA bioclimatic variable loadings from the reduced set of elevation
808 (ALT), temperature (BIO1-BIO9, and precipitation (BIO15 and BIO18) covariates. The standard
809 deviation, proportion of variance, and cumulative proportion is provided for each PC axis.

Variable	PC1	PC2	PC3	PC4	PC5	PC6	PC7	PC8
ALT	0.217	0.256	-0.629	0.352	-0.070	0.476	0.101	0.356
BIO2	0.510	0.174	-0.107	-0.499	0.197	0.336	0.011	-0.545
BIO5	0.502	-0.119	0.444	-0.166	-0.051	0.181	-0.369	0.581
BIO7	-0.161	0.552	-0.018	-0.517	0.190	-0.236	0.351	0.432
BIO8	0.432	0.249	0.326	0.292	-0.469	-0.201	0.531	-0.130
BIO9	0.136	-0.596	0.015	0.003	0.447	0.089	0.626	0.160
BIO15	-0.012	0.407	0.383	0.482	0.653	0.117	-0.081	-0.091
BIO18	0.458	-0.037	-0.378	0.125	0.265	-0.714	-0.221	0.027
Standard deviation	1.548	1.450	1.161	0.872	0.793	0.680	0.439	0.330
Proportion of variance	0.300	0.263	0.168	0.095	0.079	0.058	0.024	0.014
Cumulative proportion	0.300	0.563	0.731	0.826	0.905	0.962	0.986	1.000

810